ELSEVIER

Journal of Nuclear Materials 278 (2000) 233–241

journal of nuclear materials

www.elsevier.nl/locate/jnucmat

Electron and ion irradiation of zeolites

S.X. Wang *, L.M. Wang, R.C. Ewing

Department of Nuclear Engineering & Radiological Sciences, The University of Michigan, Cooley Bldg., 2355 Bonisteel Blvd., Ann Arbor, MI 48109-2104, USA

Received 9 February 1999; accepted 18 September 1999

Abstract

Three zeolites (analcime, natrolite, and zeolite-Y) were irradiated with 200 and 400 keV electrons. All zeolites amorphized at a relatively low electron fluence. The electron fluences for amorphization by the 200 keV electron irradiation at room temperature were: 7.0×10^{19} e^-/cm^2 (analcime), 1.8×10^{20} e^-/cm^2 (natrolite), and 3.4×10^{20} e^-/cm^2 (zeolite-Y). These doses are equivalent to an energy deposition between 2.6×10^{10} and 1.27×10^{11} Gy. An inverse temperature dependence of amorphization dose was observed for all three zeolites, i.e., amorphization dose decreased with increasing temperature. Analcime was also irradiated with 1.5 MeV Kr^+ from 300 to 973 K. The amorphization dose by the ion irradiation was constant, $\sim 1 \times 10^{14}$ ions/cm^2, which is ~ 0.1 dpa of collisional damage and $\sim 6.25 \times 10^8$ Gy of ionizing energy deposition.

PACS: 61.80.Fe; 61.80.Jh; 87.64.Dz; 82.50.Gw

1. Introduction

Zeolites are hydrous aluminosilicates. The crystal structures of the three zeolites are shown in Fig. 1 (based on structural data from Refs. [1–3]). The basic zeolite structure consists of a three-dimensional framework of $[SiO_4]$ and $[AlO_4]$ tetrahedra. The framework is generally open and contains channels and cavities in which cations and water molecules are located. The channel sizes within the structures are marked by the dash-lines in Fig. 1. The cations often have a high degree of mobility giving rise to a high ion-exchange capacity, and molecular water is readily lost and regained. Because of their 'cage-like' structures, zeolites have found many applications, such as ion-exchange media and molecular sieves catalysts. The high ion-exchange capacity of zeolites has led to their use for the removal of Cs^+, Sr^{2+} and actinides from high-level liquid nuclear waste [4–7]. Zeolites have also been proposed as back-fill material [8] and as waste forms [9] for the geological disposal of nuclear waste.

Because zeolites have a high retention capacity for radionuclides [10], they will be exposed to high-radiation doses (α- and β-decay events) in the near-field of a nuclear waste repository. Irradiation of these phases may result in changes to the crystal structure and properties, such as ion-exchange and sorption capacities. Several studies of zeolite have indicated that zeolites could be amorphized during electron irradiations [8,9,11–13]. In this study, we have completed a detailed investigation of electron and ion damage of zeolite in a temperature range from 25 to 1073 K.

2. Experimental methods

Three zeolites: analcime, natrolite, and zeolite-Y were subjected to electron irradiations. Analcime and natrolite samples are naturally occurring, and zeolite-Y is synthetic. The ideal chemical compositions of the three zeolites are: $Na_{16}Al_{16}Si_{32}O_{96} \cdot 16H_2O$ (analcime), $Na_{16}Al_{16}Si_{24}O_{80} \cdot 16H_2O$ (natrolite), and $NaAlSi_2O_6 \cdot nH_2O$ (zeolite-Y). The relative Al:Si ratios were confirmed by energy dispersive spectrometry (EDS). The

* Corresponding author. Tel.: +1-734 647 9656; fax: +1-734 647 8531.

E-mail address: shixin@engin.umich.edu (S.X. Wang).

0022-3115/00/$ - see front matter
PII: S0022-3115(99)00246-9

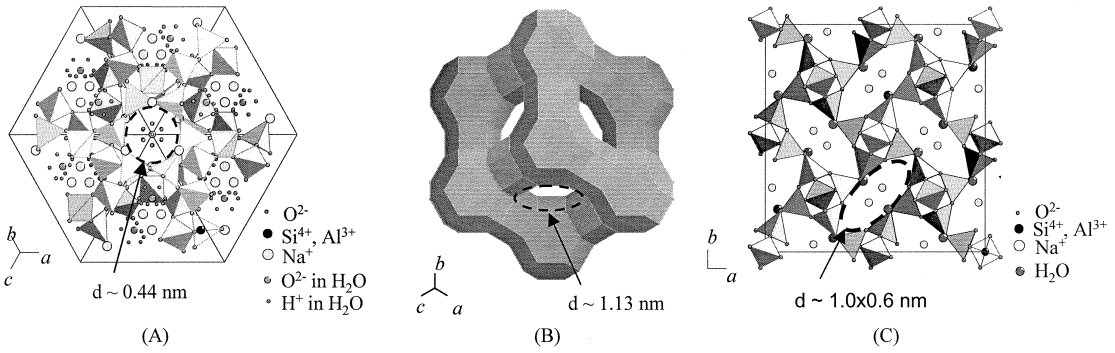

Fig. 1. (A) Crystal structure of analcime projected along [1 1 1] direction. (B) Crystal structure of zeolite-Y along [1 1 1] direction showing the cages formed by $[Si, Al]O_4$ tetrahedra. The vertices of the polygons are Si or Al. (C) Structure of natrolite looking down [0 0 1] direction. The diameters of the main channels within the structures are marked by the dash-lines.

structures of the three phases were confirmed by electron diffraction.

The 200 keV electron irradiation with in situ observation of the three zeolites was conducted using a JEM 2000FX transmission electron microscope (TEM). A heating stage was used to examine the temperature effect on the radiation damage. Samples were irradiated in a temperature range from 300 to 973 K. Analcime samples were also irradiated by 400 keV electrons with an AEI high voltage electron microscope (HVEM) at Argonne National Laboratory using a liquid helium cold stage and a tungsten heating stage. The temperature range of the 400 keV electron irradiation of analcime was 25–1073 K. The electron flux was measured by a Faraday cup (400 keV irradiation) or screen current density through a hole in the sample (200 keV irradiation). The dose rate effect was studied between 2.35×10^{17} and 2.25×10^{19} e^-/cm^2 s. During irradiation, the electron beam was spread over an area with a diameter of at least five micrometers in order to obtain a uniform beam profile in the area of observation and to reduce beam heating. High-resolution electron microscopy (HREM) was also performed using a JEM 4000EX TEM.

To compare the damage processes due to nuclear collision and due to ionization, analcime samples were also irradiated with 1.5 MeV Kr^+ from 300 to 973 K using the HVEM-Tandem Facility at Argonne National Laboratory. The dose rate was 8.5×10^{11} ions/cm^2 s. The electron microscope was operated at an accelerating voltage of 300 keV. To reduce the electron damage to the sample, the electron beam was turned off during most of the ion irradiation, and the electron beam was spread during TEM observation.

3. Results

All three zeolites transformed to the amorphous state easily under electron irradiation. Analcime was most easily amorphized. The electron fluences for amorphization of the three zeolites by 200 keV electron at room temperature were: 7.0×10^{19} e^-/cm^2 (analcime), 1.8×10^{20} e^-/cm^2 (natrolite), and 3.4×10^{20} e^-/cm^2 (zeolite-Y). The sequence of electron diffraction patterns recorded during irradiations of natrolite and zeolite-Y are shown in Fig. 2. The transformation from the crystalline-to-amorphous state was progressive. The high-resolution lattice images of zeolite-Y clearly show the gradual disruption of the periodic structure (Fig. 3). The transformation was uniform over the observed region. The dose rate effect was examined in the range of $2.35 \times 10^{17} - 2.25 \times 10^{19}$ ions/cm^2 s. Changes in the dose rate did not affect the amorphization dose significantly in the range of study.

The amorphization dose was measured at different temperatures. The variation of amorphization dose with temperature for the three zeolites is plotted in Fig. 4. For all the electron irradiations, the amorphization dose decreases with increasing temperature. The 1.5 MeV Kr^+ irradiation did not show a significant temperature effect (Fig. 4). The amorphization fluence for analcime under 1.5 MeV Kr^+ irradiation is $\sim 1 \times 10^{14}$ ions/cm^2 and is almost constant from 300 to 973 K.

Bubbles were observed in analcime and natrolite during electron irradiation. The bubbles were confirmed by sample tilting and through focus imaging with TEM observation. No bubble was observed in zeolite-Y. In analcime, bubbles formed after the sample became amorphous. In natrolite, bubble formation was concurrent with amorphization.

4. Discussion

The energy loss of electrons in materials can be calculated using electron stopping in solids. The Bethe equation for electron particle stopping is [14]

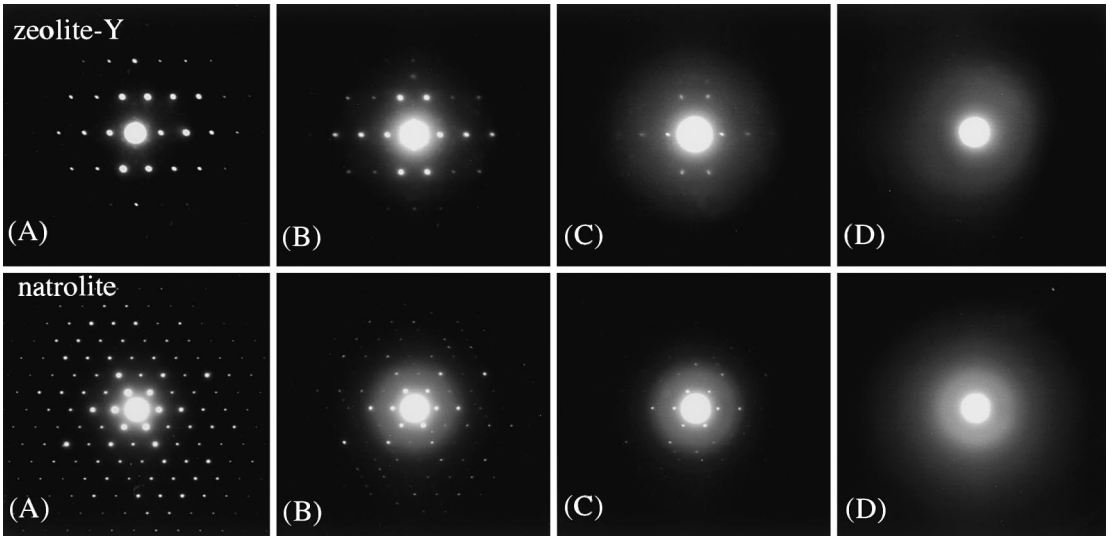

Fig. 2. The electron diffraction patterns show the progressive changes in natrolite and zeolite-Y from crystalline-to-amorphous. For natrolite, the approximate electron doses were (A) beginning of the irradiation, (B) 1×10^{20}, (C) 1.5×10^{20}, and (d) 1.8×10^{20} e^-/cm^2. For zeolite-Y, the approximate doses were (A) beginning of the irradiation, (B) 2×10^{20}, (C) 3×10^{20}, and (D) 3.4×10^{20} e^-/cm^2.

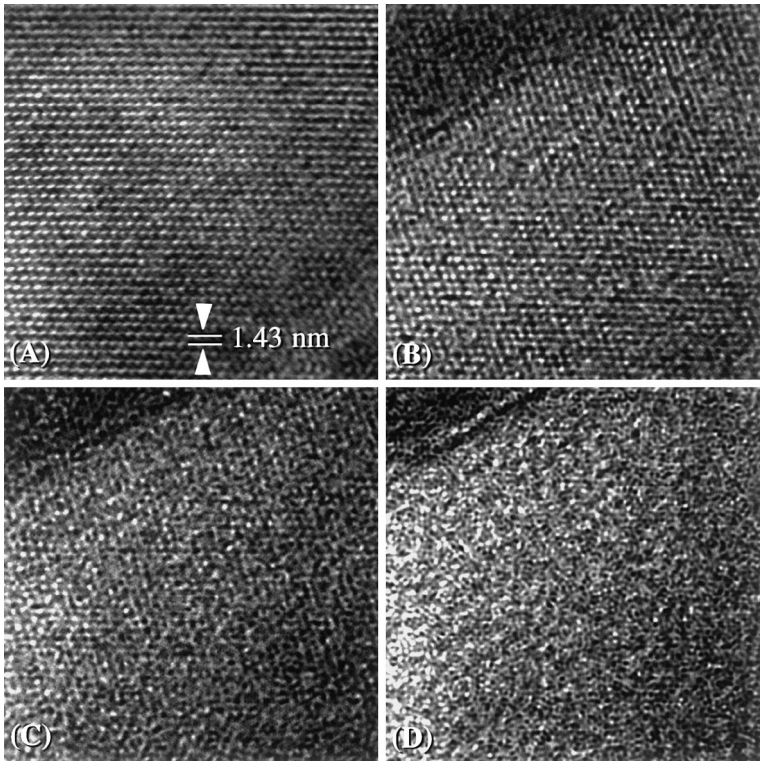

Fig. 3. HREM images of the zeolite-Y lattice show the uniform and progressive change from the crystalline-to-amorphous state under a 400 keV electron irradiation. The approximate doses were: (A) beginning of the irradiation, (B) 2×10^{20}, (C) 4×10^{20}, and (D) 6×10^{20} e^-/cm^2.

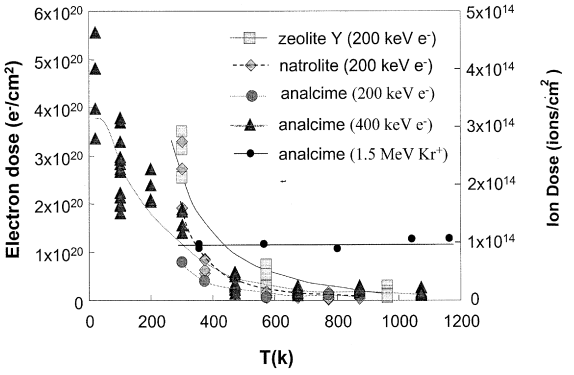

Fig. 4. Temperature dependence of amorphization dose of three zeolites. The curves were plotted according to the model detailed in the text.

$$-\frac{dE}{dx} = \frac{5.09\times10^{-25}n}{\beta^2} \times \left[\ln\frac{3.61\times10^5\tau\sqrt{\tau+2}}{I_{ev}} + F(\beta)\right] \text{MeV/cm},$$

where

$$F(\beta) = \frac{1-\beta^2}{2} + \frac{1}{2(\tau+1)^2}\left[\frac{\tau^2}{8} - (2\tau+1)\ln 2\right]. \quad (2)$$

in which $\beta = V/c$ = speed of the electron relative to speed of light in vacuum; n is the number of electrons per unit volume in the medium; $\tau = T/mc^2$ the kinetic energy, T, of the electron expressed in multiples of the electron rest energy mc^2; I_{ev} is the mean excitation energy of the medium. The following empirical formula was used to calculate the mean excitation energy [14]:

$$I \cong \begin{cases} 19.0 \quad \text{eV}, & Z = 1 \\ 11.2 + 11.7Z \quad \text{eV}, & 2 \leqslant Z \leqslant 13 \\ 52.8 + 8.71Z \quad \text{eV}, & Z > 13, \end{cases} \quad (3)$$

where Z is the atomic number of target. The composite value of I for multiple-element materials is given by

$$\ln I = \frac{1}{n}\sum_i N_i Z_i \ln I_i, \quad (4)$$

where n is the total number of electrons/cm^3 in the material.

The I value for analcime is 125.5. The stopping powers of analcime were calculated, according to Eq. (1), as 5.3 MeV/cm for 200 keV electron and 4.1 MeV/cm for 400 keV electron. Similarly, the stopping powers for other two zeolites are: 5.26 MeV/cm (200 keV, natrolite) and 4.51 MeV/cm (200 keV, zeolite-Y).

Using the stopping powers, the amorphization doses were converted to energy depositions as 2.62×10^{10} Gy (analcime), 6.74×10^{10} Gy (natrolite) and 1.27×10^{11} Gy (zeolite-Y). The amorphization dose for 400 keV electron irradiated analcime is 4.34×10^{10} Gy.

The amorphization of zeolites under electron irradiation was mainly due to ionization processes. This is because almost all of the energy loss by electron irradiation is by ionization within the energy range of this study. Displacements by nuclear collision can be estimated by the displacement cross-section for electron radiation, σ_d, which can be calculated using McKinley and Feshbach theory [15]

$$\sigma_d = (0.2495 \text{ barn})Z^2\left(\frac{1}{\beta^4\gamma^2}\right) \times \left[\left(\frac{E_m}{E_d} - 1\right) - \beta^2\ln\frac{E_m}{E_d} + \pi\alpha\beta\left\{2\left[\left(\frac{E_m}{E_d}\right)^{1/2} - 1\right] - \ln\frac{E_m}{E_d}\right\}\right], \quad (5)$$

in which

$$E_m = 2\frac{m}{M}\frac{(E+2mc^2)E}{mc^2}, \quad (6)$$

where E_m is the maximum energy transferred to target nucleus; E_d is the displacement threshold energy; Z is the atomic number; m is the mass of electron; M is the mass of target nucleus; $\beta = v/c$; v is the speed of the electron and c is the speed of light in vacuum; $\gamma = (1-\beta^2)^{-1/2}$. The number of displacements per atom, dpa, in thin target sample is related to the displacement cross-section by [16]

$$\text{dpa} = D\sigma_d, \quad (7)$$

where D is the electron dose (e$^-$/cm^2).

For a 200 keV electron irradiation on zeolites, the maximum transferred energies, E_m, to target nuclei are 525 eV (H), 32.8 eV (O), 22.8 eV (Na), 19.4 eV (Al) and 18.8 eV (Si). The cross-sections (barns) for electron radiation are calculated as: 9.6 (H), 21.3 (O), 21.2 (Na), 0 (Si), and 0 (Al), assuming $E_d = 20$ eV. Except for H, the values of E_m are too small for multiple displacements. For single displacements by electron irradiation on a compound, the average of cross-sections weighted by atomic ratio is used. The average of displacement cross-sections for electron irradiation is 10 barns for all the three zeolites. According to Eq. (7), the estimated displacements (dpa) by nuclear collision are about 0.0007, 0.0018, and 0.003 for the amorphization doses of 7×10^{19} e$^-$/cm^2 (analcime), 1.8×10^{20} e$^-$/cm^2 (natrolite), and 3.4×10^{20} e$^-$/cm^2 (zeolite-Y), respectively. Multiple displacements by H knock-on atoms (PKAs) can also be estimated. Assuming all the displaced H atoms have energy of 500 eV, using SRIM-2000, we have calculated the displacements in zeolites to be 0.008 displacements/ion/Å or 1.2 displacements/H within the range (~150 Å of 500 eV H). For about 15 mol% H in

zeolites, the displacements of H by electrons are 0.00015, 0.00038, and 0.00071 per atom. These PKAs further create displacements of 0.00018, 0.0005, and 0.0008 dpa in analcime, natrolite, and zeolite-Y. Therefore, the maximum total displacements by nuclear collision are roughly 0.0009–0.004 dpa for these three zeolites at the amorphization dose. Obviously, the displacement dose is too small to introduce significant structural damage in zeolites. This calculation confirmed that the electron damage is mainly due to ionization rather than nuclear collision.

Further support for the ionization-induced amorphization is from the comparison of 400 and 200 keV electron irradiation of analcime. The 400 keV electron has a larger displacement cross-section (Eq. (5)) and smaller ionization energy loss (Eq. (1)) than a 200 keV electron. The fact that 400 keV electron irradiation required a higher amorphization dose than that of 200 keV electron showed that the amorphization of analcime was due to ionization rather than nuclear collisions.

Simple radiolysis models of electron damage predict a uniform damage rate across an irradiated region [17–19]. The uniform transformation from the crystalline-to-amorphous state, as observed by high-resolution transmission electron microscopy (HRTEM) (Fig. 3), is consistent with a dominantly ionization process. The susceptibility of zeolites to amorphization is attributed to their open structures and their metastability. The open, cage-like structure of zeolite is susceptible to breakdown if a part of the network is disrupted. Because the zeolite structure is based on a delicate charge balance of cations and anions, removal or addition of non-network elements, such as Na^+, can also cause local distortions of the structure. Displacements within this open structure can easily be accomplished by either direct collision or ionization by an incident electron. Unbalanced charge caused by solid-state radiolysis may be the main driving force for the collapse of local structure.

The susceptibility to amorphization of most crystalline phases is based on the resistance to recrystallization [20]. However, zeolites are formed by hydrothermal alteration in nature or synthesized by hydrothermal reactions. Zeolites cannot be formed from an oxide melt. The decreasing amorphization dose with increasing temperature for all of the zeolites in this study (Fig. 4) also indicates the thermal instability of the zeolites. This showed that thermal energy assisted damage accumulation rather than annealing the damage. All three zeolites can be amorphized by heating. The amorphization temperatures are 900°C for zeolite-Y and 1000°C for analcime and natrolite. Thus, we expect that there is no driving force for the recrystallization of zeolite under electron and ion irradiations. Without annealing, the susceptibility of zeolites to amorphization is solely based on how likely the structure is to 'collapse' during irradiation. During electron irradiation, most of the energy loss is due to ionization. In zeolites, the most probable displacements caused by ionization are the light and loosely bonded species, such as Na^+, H^+ and water molecules. These species can be easily displaced by ionization or by direct collision. The structural water may be either displaced as a molecule or as separate ions and radicals. During ionizing irradiation, different transient radicals are produced, and electrons (e^-) and electron holes (h^+) can be trapped by ion clusters and other aggregates. The typical radicals or ion clusters include: $(OH)^-$, $(H_2O)_n^-$, H^+, $Na_n^{(n-1)+}$, Z^+ [21,22], where Z is the zeolite framework. The radicals are mobile due to local charge imbalance. These radicals may further interact with the zeolite $[Al,Si]O_4$ framework and induce the collapse of the structure. The ionization and decomposition of water molecules (i.e., the production of $(H_2O)_n^-$, $(OH)^+$, H^+) is the dominant process in the electron irradiation of zeolites, because the water content can be as high as 50% of the total volume of zeolites. The water molecule is also highly mobile due to ionization because it is bonded to structure only by van der Waals forces. During the electron irradiation, the $[Al,Si]O_4$ framework may collapse due to several mechanism (Fig. 5), as suggested in previous studies [18,19]:

1. Direct removal of network atoms. This has a low probability due to the strong bonding in the network.
2. The breaking of the [Al,Si]–O bonds due to the removal of Na^+ by either direct ionization of Na^+ or by the $(OH)^-$ radical.
3. The breaking of the [Al,Si]–O bond due to the formation of and O–H bond by H^+.

If the structure has large enough openings, some of the radiation-induced mobile radicals are easily released without disrupting the framework structure. Some radicals can also recombine (such as $e^- + h^+$ and $OH^- + H^+$) without interacting with the zeolite framework. This is the case for zeolite-Y. In zeolite-Y, the largest free aperture diameter of the channel is

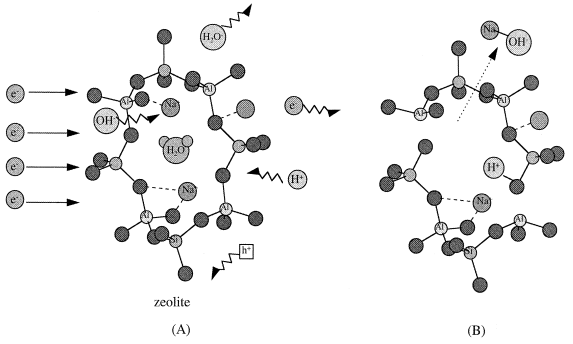

Fig. 5. Schematic diagram of the mechanisms of structural damage of zeolite structure by electron irradiation.

1.13 nm (Fig. 1), which provides a large 'window' for the movement of radicals. In comparison, the aperture sizes of analcime and natrolite are 0.44 and 1×0.6 nm (Fig. 1), respectively. Thus, the release and recombination rates of radiation-induced radicals from analcime and natrolite are not as rapid as that in zeolite-Y. More free radicals are available to cause the disruption of the framework structure in analcime and natrolite. This explains why zeolite-Y requires the largest dose for amorphization. Between analcime and natrolite, the aperture size in analcime is smaller than that of natrolite, thus the radical release and recombination rate in analcime is slower, leading to a higher damage rate.

This hypothesis is supported by the observation of bubble formation in analcime and natrolite (Fig. 6(A) and (B)). In zeolite-Y, no bubbles were observed (Fig. 6(C)), even under the focused electron beam. The bubbles may be due to the accumulation of water. Molecular hydrogen, as reported in the γ-radiation of zeolites [23], may be another source for bubble formation. In zeolite-Y, the release rate of water was so rapid that not enough water molecules can accumulate to form bubbles. In analcime and natrolite, the water molecules and other radicals were not completely released. The water molecules accumulate locally to form bubbles. The bubbles in analcime formed only following prolonged irradiation after amorphization (except under the very intense focused beam that causes almost instant bubble formation after amorphization). The shape of the bubbles in analcime is rounded because they are formed in a uniformly amorphous matrix. In natrolite, the bubbles formed at much lower dose than that required for amorphization. The shape of the bubbles in natrolite is irregular in contrast to the round bubbles in analcime. The possible explanation to the irregularly shaped bubbles in natrolite is that the bubbles formed within a crystalline matrix.

In summary:

1. The water migration and release rate in analcime is so low that even bubbles cannot form in short time. The free radicals interact with the framework causing structural disruption. Because the water was not released, the water molecules eventually formed bubbles in the amorphous matrix after prolonged irradiation.
2. The water release rate in natrolite was faster than that of analcime, but not fast enough to be fully released from the sample to prevent bubble formation. Bubbles formed while the sample was being amorphized.
3. Because of the larger channel size in zeolite-Y, molecular water was almost instantly released during irradiation. Thus, no bubbles formed even under prolonged irradiation. Because of the faster release of water and recombination of various radicals in zeolite-Y, a larger fraction of the absorbed energy is not utilized in the disruption of the framework structure. Thus, the amorphization dose for zeolite-Y is higher.

At elevated temperature, a decrease in the amorphization dose was observed (Fig. 4) with electron irradiation. This observation is based on three series of irradiations using 200 keV electrons from 300 to 973 K and one series of irradiations using 400 keV electrons from 25 to 1073 K. This temperature dependence is the inverse of that commonly observed for irradiation-induced amorphization of crystalline solids which usually show an increased amorphization dose at elevated temperatures. A similar dose–temperature relationship has been reported in an electron irradiation study of coesite [24], in which the electron dose decreased with increasing temperature. The explanation of this observation was that these phases are thermally unstable. Almost all zeolites become amorphous or transform to other phases upon heating [25–28].

Based on these results, we suggest that the thermal energy due to sample heating enhances the extent of

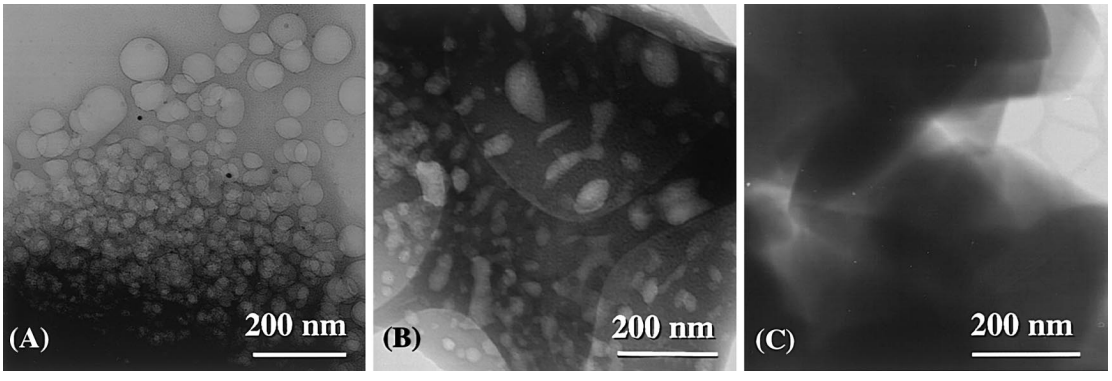

Fig. 6. The 200 keV electron irradiation at room temperature produced bubbles in analcime (A) and natrolite (B). No bubbles were formed in zeolite-Y (C).

damage caused by the incident electrons. Thermal energy assists the electron beam damage by:

1. increasing the excitation of moving species (Na^+, OH^-, H^+, $(H_2O)_n^-$, etc.),
2. decreasing the stability of the $[(Si, Al)O_4]$ network due to thermal vibrations,
3. enhancing the radiolytic reactions that disrupt the $[Al,Si]O_4$ network.

A simple empirical model has been developed to follow the dose–temperature trend. In this model, we assume that there is no recovery of damage. We define the initial temperature, T_1, as the temperature above which thermal energy begins to contribute to the damage, and, the critical temperature, T_2, as the temperature above which the material becomes amorphous without irradiation. We define the temperature effect using an exponential term, $\exp(-Q/T)$, in which Q is the activation energy (in units of temperature).

The damage rate equation is written as

$$\frac{df_c}{dD} = \frac{-f_0(1-f_c)}{1-\exp(-Q/T)}, \tag{8}$$

where f_c is the crystalline fraction in the irradiated region; D the electron dose; and f_0 is the amorphous fraction created by a unit of electron dose. This is a semi-empirical equation. The effect of thermal energy is to extend the damaged region. The parameter Q can be thought of as an energy barrier that prevents the damage for extending beyond the original damage region, defined as the damage region at 0 K. The solution to Eq. (8) is

$$f_c = 1 - \exp\left(\frac{-f_0}{1-\exp(-Q/T)}D\right), \tag{9}$$

which gives the change of crystalline fraction as a simple exponential function of electron dose. The amorphization dose is then

$$D_c = K[1-\exp(-Q/T)], \tag{10}$$

where D_c is the amorphization dose and K is a constant. With the addition of initial conditions, $D_c = D_0$ when $T \leqslant T_1$ and $D_c = 0$ when $T = T_2$:

$$D_c = \begin{cases} D_0 \quad \text{for } T \leqslant T_1, \\ D_0\left[1-\exp\left(-Q\cdot\left(\frac{1}{T-T_1}-\frac{1}{T_2-T_1}\right)\right)\right] \\ \quad \text{for } T_1 < T \leqslant T_2. \end{cases} \tag{11}$$

This is the temperature dependence of amorphization dose for the electron irradiation of zeolite. The general form of Eq. (11) is plotted in Fig. 7. The curves based on the experimental data for electron irradiations in Fig. 4 were also plotted using Eq. (11). The model described by Eq. (11) provides a successful fit to the experimental data. The activation energies, Q, obtained for Fig. 4 are 40 K for the natrolite data and 100 K for the other two

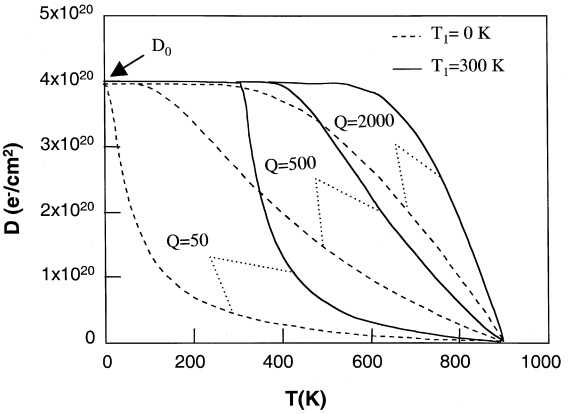

Fig. 7. Temperature dependence of amorphization dose of zeolite under electron irradiation according to Eq. (11) where T_2 is 900 K. Two sets of curves (solid- and dash-lines) show the cases of T_1 as 0 and 300 K. The curves within one set show the change with Q.

zeolites. If we use the form $Q = E_a/k_B$, where k_B is the Boltzmann constant, E_a is 0.0034 eV for 200 keV electron irradiation of natrolite and 0.0086 eV for the other data. These activation energies are very small as compared with the activation energies for many other processes (for example, ~ 0.1 eV for H-diffusion in metal and ~ 2 eV for vacancy formation [29]). The underlying physical meaning of the activation energy, Q, requires further investigation. Due to the difficulty of effectively cooling powder samples, low temperature (< 300 K) data on powder samples of zeolite-Y and natrolite are presently not available.

The ion irradiation did not show a significant temperature effect (Fig. 4). Compared with the results from the electron irradiations, this result revealed a significant difference between the cascade damage and ionization damage. The energy loss by nuclear collision or ionization can be calculated using the Monte Carlo code SRIM-2000 [30]. The calculation was based on the assumption of a displacement energy of 20 eV. For an amorphization dose of 1×10^{14} Kr^+/cm^2, the collisional damage is 0.1 dpa (displacement per atom) and the energy loss by ionization is 6.25×10^8 Gy. Compared with the electron irradiation, the ionizing energy loss for the amorphization dose of the Kr^+ irradiation is only 2% of that of the 200 keV electron irradiation at room temperature. This suggests that the amorphization by Kr^+ irradiation is mainly due to nuclear collisions. In the heavy ion irradiation, the incident ion disrupts the structure by the formation of displacement cascades. Within the initial period of cascade (or subcascades) formation, all the atoms in the cascade can be considered as being in a liquid or gaseous state [20]. Without recrystallization, such as in the case of zeolite, the whole volume of the cascade becomes amorphous upon energy

dissipation. The total dose for the 'full' amorphization of the TEM sample depends on the size of the cascade. In ion irradiations, the size of the cascade is determined mainly by the ion mass, ion energy, and the displacement energy of the target material, and it is relatively independent of sample temperature. This is because the energy density within a cascade is much higher than the thermal energy contribution. Thus, for heavy ion irradiation, increasing temperature does not have as significant effect on zeolite as does the electron irradiation.

The model described by Eq. (11) is mainly for ionizing irradiation. The model is based on an ionization process for which the damaged regions are considered to be in a low energetic state as compared with the high energy density in a displacement cascade under heavy ion irradiation. This is a reasonable assumption for the electron irradiation, for which no dense cascade forms in the range of the energy and dose rate used in this study. The ionization damage process is susceptible to the temperature increase because of the direct interaction of free radicals with the $[Al, Si]O_4$ network. In contrast, the damage created by a heavy ion in cascades or subcascades may consist of several thousands atoms in collaborative movement. The moving species, which are mainly the displaced atoms, only interact with the matrix at the subcascade boundaries. Thus, we anticipate that the damage caused by a displacement cascade is less easily affected by the increase of sample temperature than in the case of the ionization process. If we apply Eq. (11) to the results of the 1.5 MeV Kr^+ irradiation of analcime, the startup temperature, T_1, must be higher than 973 K. The amorphization dose of 1.5 MeV Kr^+ in Fig. 4 is actually a flat line at $T < T_1$ as shown in Fig. 7.

The radiation-induced amorphization of zeolite may have a positive consequence in terms of retaining radioactive elements. The dose rate in this study is 10^8–10^9 higher than that experienced by radionuclide-containing zeolites. However, we did not observe a dose rate effect in the range of $2.35 \times 10^{17} - 2.25 \times 10^{19}$ e^-/cm^2 s. The results of this study provide insight into the effects of ionizing radiation on zeolite structures over long period. The amorphization of zeolite has been known to reduce the release of absorbed cesium, strontium and thorium during leaching tests [26,31]. Amorphization also retards molecular/elemental uptake and reduces the sorption capacity of zeolites [31,32]. The effect of electron irradiation on zeolite suggests the possible closure of structural channels, at least to a certain degree, during the irradiation. An estimate of the time required for the full amorphization of zeolites with a specific radionuclide loading due to the radioactive decay can be made. For a 10 wt% ^{137}Cs loading in analcime, the time required to reach the amorphization dose is 400 years, and much less, 50 years, for a full loading (replacement of all of the Na^+ with Cs^+, 41 wt%). In our experiments, we observed a gradual growth of amorphous fraction during irradiation. Thus, localized amorphization due to β-decay events may occur much earlier than the time required for the full amorphization of the bulk material. Because radiation occurs only after radioactive elements are absorbed into the zeolite structure, the radiation damage may effectively close the pathways for further release of radionuclides.

5. Conclusions

We have investigated electron-irradiation effects on three zeolites: analcime, natrolite and zeolite-Y. All three zeolites amorphized easily upon irradiation. Analcime was the most easily amorphized, and the zeolite-Y required the largest electron dose to become fully amorphized. The different susceptibilities of these three zeolites to amorphization were attributed to the different sizes of the channels in the zeolite structures, through which the radiation-induced radicals can escape and recombine. The different channel sizes also affected bubble formation. For the zeolite with largest channel (zeolite-Y), no bubbles formed because of the rapid release of water. For analcime, which has the smallest channels, the water accumulation was so slow that the bubbles formed only after complete amorphization. Bubbles formed in natrolite prior to complete amorphization. With increasing temperature, the amorphization doses of the three zeolites decreased. This amorphization dose–temperature relationship was modelled based on the thermal instability of the zeolites. Analcime samples were also irradiated with 1.5 MeV Kr^+ from 300 to 973 K. The amorphization dose of the Kr^+ irradiation was constant over the range of temperatures.

Acknowledgements

The electron irradiation and TEM analysis were conducted at the Electron Microbeam Analysis Laboratory at the University of Michigan and at the HVEM-Tandem Facility of Argonne National Laboratory. This work was supported by the Department of Energy's Environmental Management Science Program (DE-FG07-97ER45652).

References

[1] G. Ferraris, D.W. Jones, J. Yerkess, Z. Kristallogr. 135 (1972).
[2] P.K. Maher, F.D. Hunter, J. Scherzer, in: E.M. Flanign, L.B. Leonard (Eds.), Molecular Sieve Zeolites, Washington, 1971, p. 266.
[3] D.R. Peacor, Am. Min. 58 (1973) 676.

[4] I.I. Ames, Am. Min. 45 (1960) 689.
[5] H. Mimura, K. Akiba, K. Kawamura, J. Nucl. Sci. Technol. 31 (1994) 463.
[6] I. Nava, I. Garcia-Sosa, M. Solache-Rios, J. Radio. Nucl. Chem. 191 (1995) 83.
[7] R.K. Ahluwalia, H.K. Geyer, J.P. Ackerman, Indust. Eng. Chem. Res. 37 (1998) 145.
[8] L.M. Wang, S.X. Wang, R.C. Ewing, Proceedings of the International Conferance on High-Level Radio. Waste Manag. Conf. (1998) 772.
[9] B.G. Storey, T.R. Allen, Mater. Res. Soc. Symp. Proc. 481 (1998) 413.
[10] R.T. Pabalan, J.D. Prikryl, P.M. Muller, T.B. Dietrich, Mater. Res. Soc. Symp. Proc. 294 (1993) 777.
[11] M. Pan, Micron 27 (1996) 219.
[12] Y. Yokota, H. Hashimoto, T. Yamaguchi, Ultramicroscopy 54 (1994) 207.
[13] Y. Bando, Inst. Phys. Conf. Ser. 93 (1988) 131.
[14] J.E. Turner, Atoms, Radiation, and Radiation Protection, McGraw-Hill, New York, 1992, pp. 78, 88–89.
[15] J.W. Corbett, in: F. Seitz, D. Turnbull (Eds.), Solid State Physics, vol. 7, Academic Press, New York, 1966, p. 20.
[16] M. Nastasi, J.W. Mayer, J.K. Kirvonen, Ion–solid Interactions: Fundamentals and Applications, Cambridge University, Cambridge, UK, 1996, p. 166.
[17] E.H. Hirsch, Nature 293 (1981) 759.
[18] L.W. Hobbs, in: G.W. Bailey (Ed.), Proceedings of the 41st Annual EMSA Meeting, San Francisco Press, San Francisco, CA, 1983, p. 346.
[19] M.M.J. Treacy, J.M. Newsam, Ultramicroscopy 23 (1987) 411.
[20] S.X. Wang, L.M. Wang, R.C. Ewing, R.H. Doremus, J. Non-Cryst. Solids 238 (1998) 214.
[21] G. Zhang, X. Liu, J.K. Thomas, Radiat. Phys. Chem. 51 (1998) 135.
[22] D.W. Werst, P. Han, A.D. Trifunac, Radiat. Phys. Chem. 51 (1998) 255.
[23] M. Aoki, T. Nakayama, C. Nakazato, T. Masuda, Bull. Chem. Soc. Jpn. 65 (1992) 140.
[24] W.L. Gong, L.M. Wang, R.C. Ewing, J. Zhang, Phys. Rev. B 54 (1996) 3800.
[25] I.A. Bewlistsky, B.A. Fursenko, S.P. Gabuda, O.V. Kholdeev, Y.V. Seryotkin, Phys. Chem. Min. 18 (1992).
[26] P.K. Sinha, V. Krishnasamy, J. Nucl. Sci. Technol. 33 (1996) 333.
[27] C. Kosanovic, B. Subotic, Microporous Mater. 12 (1997) 261.
[28] R. Dimitrijevic, A. Kremenovic, V. Dondur, M. Tomasevic Canovic, M. Mitrovic, J. Phys. Chem. B 101 (1997) 3931.
[29] D.R. Olander, Fundamental Aspects of Nuclear Reactor Fuel Elements, National Technical Information Service, Springfield, VA, 1976.
[30] J.F. Ziegler, J.P. Biersack, U. Littmark, The Stopping and Range of Ions in Solids, Pergamon, New York, 1985.
[31] B.X. Gu, L.M. Wang, R.C. Ewing, J. Nucl. Mater 278 (2000) 64.
[32] M. Bulow, P. Struve, Characterization of Porous Solids III 87 (1994) 551.